GA–A27959

SUPER H-MODE: THEORETICAL PREDICTION AND INITIAL OBSERVATIONS OF A NEW HIGH PERFORMANCE REGIME FOR TOKAMAK OPERATION

by

P.B. SNYDER, W.M. SOLOMON, K.H. BURRELL, A.M. GAROFALO,
B.A. GRIERSON, R.J. GROEBNER, A.W. LEONARD, R. NAZIKIAN, T.H. OSBORNE,
E.A. BELLI, J. CANDY, and H.R. WILSON

SEPTEMBER 2014

GENERAL ATOMICS

DISCLAIMER

GA–A27959

SUPER H-MODE: THEORETICAL PREDICTION AND INITIAL OBSERVATIONS OF A NEW HIGH PERFORMANCE REGIME FOR TOKAMAK OPERATION

by
P.B. SNYDER, W.M. SOLOMON,* K.H. BURRELL, A.M. GAROFALO,
B.A. GRIERSON,* R.J. GROEBNER, A.W. LEONARD, R. NAZIKIAN,* T.H. OSBORNE,
E.A. BELLI, J. CANDY, and H.R. WILSON†

This is a preprint of a paper to be presented at the Twenty-Fifth IAEA Fusion Energy Conf., October 13-18, 2014 in Saint Petersburg, Russia, and to be published in the *Proceedings*.

*Princeton Plasma Physics Laboratory, Princeton, New Jersey.
†York Plasma Institute, University of York, Heslington, York, United Kingdom.

Work supported in part by
the U.S. Department of Energy
under DE-FG02-95ER54309, DE-FC02-04ER54698,
and DE-A02-09CH11466

GENERAL ATOMICS PROJECT 03726
SEPTEMBER 2014

GENERAL ATOMICS

Super H-Mode: Theoretical Prediction and Initial Observations of a New High Performance Regime for Tokamak Operation TH/2-2

P.B. Snyder[1], W.M. Solomon[2], K.H. Burrell[1], A.M. Garofalo[1], B.A, Grierson[2], R.J. Groebner[1], A.W. Leonard[1], R. Nazikian[2], T.H. Osborne[1], E.A. Belli[1], J. Candy[1], and H.R. Wilson[3]

[1]*General Atomics, PO Box 85608, San Diego, CA 92186-5608, USA*
[2]*Princeton Plasma Physics Laboratory, PO Box 451, Princeton, NJ 08543-0451, USA*
[3]*York Plasma Institute, University of York, Heslington, York, UK*
email: snyder@fusion.gat.com

Abstract: A new "Super H-mode" regime (Fig. 1) is predicted, which enables pedestal height and predicted fusion performance substantially higher than for H-mode operation. This new regime exists due to a bifurcation of the pedestal pressure, as a function of density, that occurs in strongly shaped plasmas above a critical density. The Super H-mode regime is predicted to be accessible by controlling the trajectory of the density, and to increase fusion performance for ITER, as well as for DEMO designs with strong shaping. A set of experiments on DIII-D has identified the predicted Super H-Mode regime, and finds pedestal height and width, and their variation with density, in good agreement with theoretical predictions from the EPED model. The very high pedestal enables operation at high global beta and high confinement, including the highest normalized beta achieved on DIII-D with a quiescent edge.

1. Introduction

The pressure at the top of the edge transport barrier (or "pedestal height") strongly impacts global confinement and fusion performance of tokamaks, with fusion power production expected to scale approximately with the square of the pedestal height. The EPED model [1-3] has been developed to predict the pedestal height and width, and has been successfully tested in numerous experiments, including several cases in which predictions were made before the experiment was conducted. Development of the EPED model is ongoing, for example to include more accurate calculations of the neoclassical bootstrap current, and to incorporate the effects of multiple impurity species. Here we focus on applying the EPED model to understand and optimize the pedestal, including the notable prediction, and experimental discovery, of the "Super H-Mode" regime, which sits above the usual H-Mode pedestal root (Fig 1). Section 2 gives a brief introduction to the EPED model and describes its validation on several experiments, including studies of the important parametric dependencies of the pedestal. Section 3 describes the intertwined dependencies on density and shape that lead to the splitting of the pedestal root, and prediction of the Super H-Mode regime, at high density and strong shaping. Section 4 describes experiments on DIII-D which have successfully accessed the very high pedestal Super H-Mode regime, and begun to demonstrate its potential for enabling high confinement and high global beta, compatible with a steady, quiescent edge. Section 5 discusses prospects for Super H-Mode operation in ITER, and directions for future study.

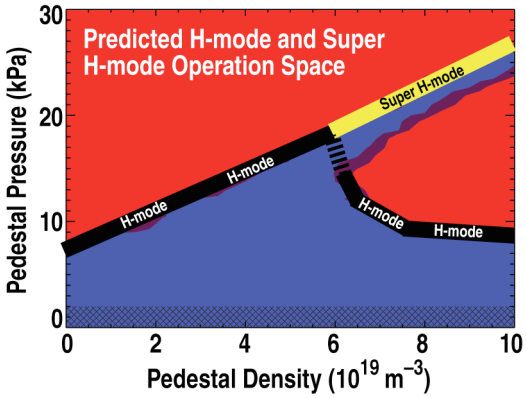

Fig 1. The Super H-mode regime (yellow) is predicted for strongly shaped plasmas above a critical density (for weakly shaped plasmas the black H-mode curve is continuous and more flat). Very high pedestal pressure and fusion performance is predicted in this regime.

2. The EPED Model: Experimental Tests and Parametric Dependencies

The EPED model [1–3] predicts the H-mode pedestal height and width based upon two fundamental and calculable constraints: 1) onset of non-local peeling-ballooning (P-B) modes at low to intermediate mode number, 2) onset of nearly local kinetic ballooning modes (KBM) at high mode number. Calculation of these two constraints allows a quantitative prediction of both pedestal height and width [Fig. 2(a)]. Both constraints are calculated directly, including important kinetic effects, with no free or fit parameters. The EPED model has been successfully compared to numerous experiments, including detailed parametric studies [e.g. Fig. 2(a)]. A comparison across 288 cases from 5 tokamaks [1–6] finds a ratio of predicted to observed pedestal height of 0.99±0.21, with a correlation of 0.91, consistent with ~10%–15% measurement uncertainty and model accuracy to within ~15%–20% [Fig. 2(b)]. High resolution pedestal diagnostics are needed to accurately measure the width of the typically narrow pedestal region, and compare to model predictions. A recent upgrade to the Thomson scattering system on DIII-D has enabled very accurate width measurement, and a comparison of measured widths to EPED predictions [Fig. 2(c)] finds a similar level of agreement (~20%) as is found in the height comparison. EPED predictions for the ITER baseline pedestal height and width are shown by black diamonds in Figs. 2(b,c). Note that while the predicted pedestal pressure for ITER is larger than that found on any existing tokamak, the predicted Troyon normalized pedestal height ($\beta_{N,ped}$) and normalized width [Fig. 2(c)] are both in the range typical of that predicted and observed for existing experiments with similar shape, aspect ratio, collisionality and q_{95}. (ITER pedestal variation with density will be discussed in Sec. 5.)

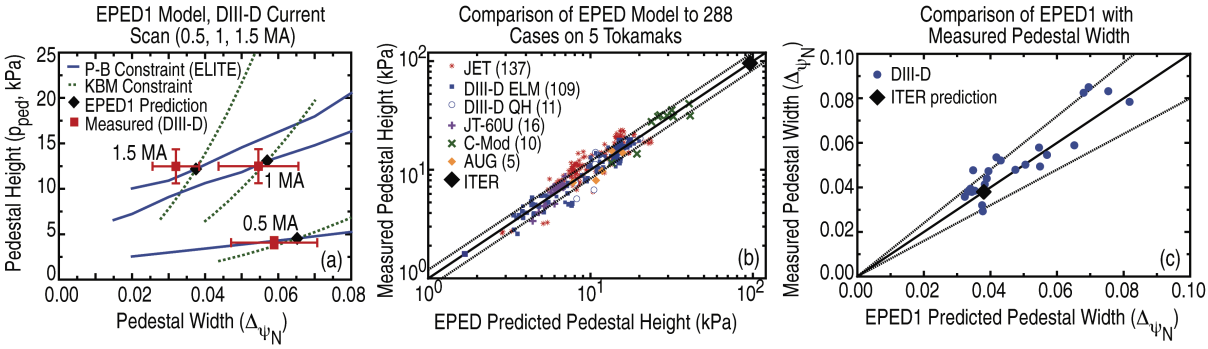

Fig. 2. (a) The EPED model predicts the pedestal height and width (black diamonds) from the intersection of calculated P-B (solid blue line) and KBM (dotted green line) constraints. Predictions for a current scan on DIII-D are found to be in good agreement with observations (red squares). (b) Comparison of EPED predictions to observed pedestal height for 288 cases on 5 tokamaks, with ITER baseline prediction also shown (black diamond). (c) Comparison of EPED predictions to pedestal width measured with high resolution Thomson scattering on DIII-D, with ITER baseline pedestal width prediction also shown (black diamond).

The combination of P-B and KBM physics in the EPED model leads to strong predicted dependence of the pedestal height on poloidal field (B_p), toroidal field (B_t) and plasma shape. These dependencies have been successfully tested in several experiments, for example an experiment on DIII-D in which the plasma current (I_p, proportional to B_p) was varied by a factor of three at fixed B_t and plasma shape [Fig. 2(a)], and a set of experiments in which both B_t and I_p were varied at high and low triangularity [Fig. 3(a)]. Broadly, a near linear increase in pedestal height with B_t*B_p is predicted [dashed lines in Fig. 3(a)], though this weakens at lower q_{95}, as can be seen in the 1.5 MA case in Fig. 2(a). Hence the Troyon normalized $\beta_{N,ped}$, defined to be the usual Troyon β_N with the average pressure replaced by pedestal pressure, is a useful figure of merit. The pedestal pressure is generally optimized at

high B_t and B_p, moderate q, and strong shaping, though complex interdependencies, particularly of shape with density, are significant, as discussed below.

An important dependence on density derives primarily from the dependence of the bootstrap current on collisionality. At low density, the pedestal is typically limited by current-driven instabilities, and the predicted and observed pedestal height increases with density (because the bootstrap current at a given pressure gradient decreases with collisionality), as shown for example in Fig. 3(b) (experiments described in Ref. 7). At higher density, bootstrap current is suppressed by high collisionality, the pedestal becomes primarily limited by pressure driven modes, and the predicted pedestal height decreases with density, as in Fig. 3(c) [from a C-Mod similarity experiment on DIII-D, described in Refs 5 and 6]. There is a strong interlinking of this density dependence with the shape dependence of peeling-ballooning stability, which will be discussed in the next section. The collisionality dependence of the bootstrap current is critical, and can be accurately assessed with the NEO kinetic code [8], which incorporates multiple ion species and the full-linearized Fokker-Planck collision operator, both for direct calculations and to assess the accuracy of simpler bootstrap current models.

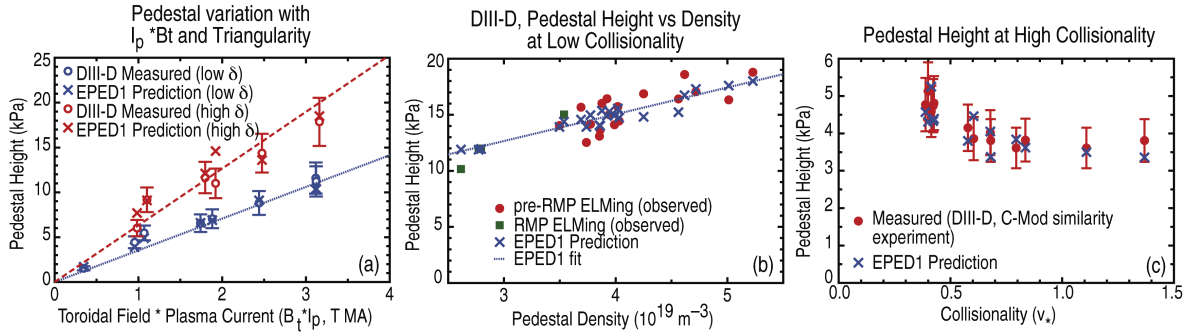

Fig. 3. (a) DIII-D observed (circles) and EPED predicted (crosses) pedestal height variation with the product of toroidal field and plasma current, shown at high triangularity (red, δ~0.55) and low triangularity (blue, δ~0.22). (b) DIII-D observed (circles and squares) and EPED predicted (crosses) pedestal height increases with density at low values of the density. (c) DIII-D observed (circles) and EPED predicted (crosses) pedestal height decreases with collisionality (i.e. with density) at high values of the collisionality (i.e. high density).

3. The Super H-Mode Regime

As discussed in Sec. 2, there is a strong dependence of pedestal height on plasma shape, due to the impact of shaping on peeling-ballooning mode stability. In particular, strong shaping leads to a partial decoupling of current-driven and pressure-driven instabilities, leading to a "nose" in the typical peeling-ballooning stability diagram [Fig. 4(b), δ=0.2 case]. Furthermore, there is a non-monotonic dependence of the pedestal height on density [e.g. Figs 3(b,c)]. More precisely this is a dependence on collisionality, which scales like the product of density and the square root of the effective ion charge Z_{eff} (at a given pressure), due primarily to the impact of collisionality on bootstrap current, and the dual role of current in driving kink/peeling modes while partially stabilizing pressure-driven modes. The shape and density dependencies are deeply inter-linked, in a way that can lead to complex behavior, including the emergence of the Super H-mode regime at strong shaping and high density.

To explore these interdependencies, we employ the EPED1 model to self-consistently predict the pedestal height and width as a function of pedestal density, for a range of plasma shapes (varying triangularity). Here we choose fixed EPED input parameters for B_t=1.9 T, I_p=1.5 MA, R=1.66 m, a=0.6 m, elongation=1.89, Z_{eff}=2.7, β_N=1.8, and do calculations for a range of pedestal density ($n_{e,ped}$=1-10 10^{19} m^{-3}) and triangularity (δ=0.0-0.5) values. Note that

each point along the solid lines on Figs 4 through 7 represents a complete EPED calculation, which self-consistently determines both pedestal height and width, though only height is shown in the figures. Figure 4(a), for example, shows the results of 57 separate EPED predictions (3 triangularity values, 19 pedestal density values), each of which in turn required roughly 400 peeling-ballooning stability calculations with ELITE across a range of toroidal mode numbers (here n=5, 6, 8, 10, 15, 20, 30, 40) on sets of model equilibria.

Predictions of pedestal height vs. pedestal density for three different values of the triangularity (δ=0.0, 0.2, 0.4) are shown in Fig. 4(a). At the lowest triangularity (δ=0, red line), the predicted pedestal height varies only mildly with density. At δ=0.2 (blue line), there is a notable increase in pedestal height with density at low density, peaking at $n_{e,ped}$~ $3.5x10^{19}$ m^{-3}, and then decreasing markedly for values above ~5. At δ=0.4 (black line), the behavior is much more complex. There is again an increase in pedestal height with density at low values of density, but the increase is much steeper than in the lower triangularity cases. The height continues to increase with density up to $n_{e,ped}$~$5.7x10^{19}$ m^{-3}, and then the solution becomes multi-valued (3 separate solutions for pedestal height at each value of pedestal density) for $n_{e,ped}$~5.7-$8x10^{19}$ m^{-3}. At high density (>$8x10^{19}$ m^{-3}), the solution again becomes single-valued.

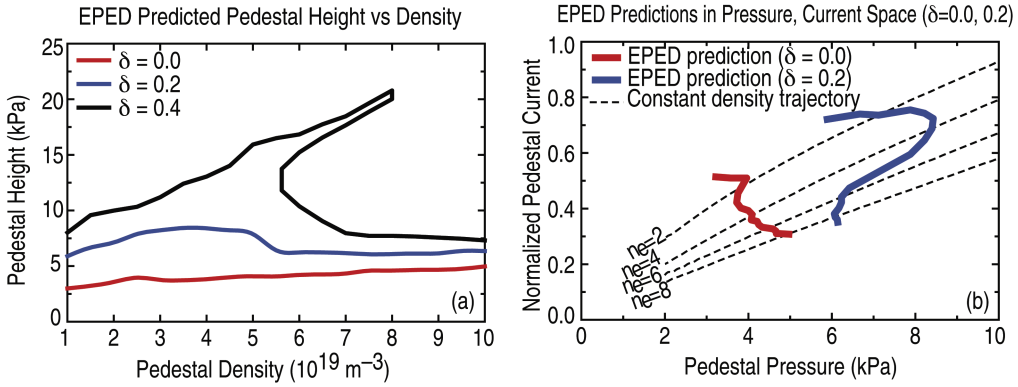

Fig. 4. (a) EPED predictions for the pedestal height (pressure in kPa) shown as a function of pedestal density for three different triangularities (0.0, 0.2, 0.4). Note that for the highest triangularity (0.4, black line) the solution becomes multi-valued for a range of densities from 5.7-$8x10^{19}$ m^{-3}. (b) The triangularity 0.0 and 0.2 cases from (a) are re-plotted in terms of pedestal current vs pedestal pressure. Trajectories of constant pedestal density are shown with dashed lines ($n_{e,ped}$=2, 4, 6, $8x10^{19}$ m^{-3}), indicating how the interaction of peeling-ballooning (+KBM) stability in pressure-current space, with the variation of current with density, leads to the dependence shown in Fig. 4(a) for the triangularity 0.0 and 0.2 cases.

To understand this behavior, including the splitting of the pedestal height solution into 3 separate roots, and formation of an (inverted) S-curve, we consider the EPED predictions in pedestal current vs pressure space, starting with the two single-valued cases (δ=0.0, 0.2), as shown in Fig. 4(b). The red and blue lines in Fig. 4(b) show the same EPED predictions as in Fig. 4(a), but plotted now in pedestal current vs pedestal pressure space. This is a similar space to that typically shown for peeling-ballooning stability diagrams, such that current driven kink/peeling modes will be limiting above, and pressure driven ballooning modes to the right. [However, note that rather than the fixed pedestal width generally used in such diagrams, this diagram shows self-consistent EPED predictions, where the pedestal width is separately predicted (and varies) at each point.] Trajectories of constant pedestal density are shown by dashed lines. For the lowest triangularity (0.0), current-driven modes are limiting only at very low density (<$2x10^{19}$ m^{-3}), and there is relatively little variation in pressure with current, due to very strong peeling-ballooning mode coupling. At higher triangularity (0.2, blue line), the current-driven and pressure driven instabilities become somewhat de-coupled,

resulting in a "nose" in the diagram, with higher pedestal pressure accessible at intermediate current (corresponding to intermediate $n_{e,ped}$~3-5x10^{19} m^{-3}). Note that the "nose" is amplified by the EPED model (from what it would be with peeling-ballooning calculations at fixed pedestal width), because the KBM constraint in EPED results in a pedestal width that increases with pressure, leading to the significant variation in pedestal height with density shown in Fig. 4(a) (blue line). Because each of the dashed lines in Fig. 4(b) intersects the red and blue curves at only a single point, the solutions for pedestal height vs density are single valued for these cases.

Now consider a case where the EPED solution becomes multi-valued, specifically a high triangularity (δ=0.5) case where the splitting of the root is pronounced over a broad range of density. The predicted pedestal height vs pedestal density for this case is shown in Fig. 5(a). Note that the root becomes multi-valued for $n_{e,ped}$>5.5x10^{19} m^{-3}, and that the high pedestal roots become strongly separated from the low pedestal root at high density. Plotting these results in pressure vs current space [Fig. 5(b)] it is clear that, due to high triangularity, the current-driven and pressure-driven instabilities have become strongly decoupled, leading to a very extended, thin "nose" in Fig. 5(b). Due to the amplifying effect of the EPED model (width increasing with height), the "nose" is so extended that it extends beyond the pressure range shown [i.e. the upper and lower green lines in Fig. 5(b) are disconnected throughout the range shown, unlike the two cases in Fig. 4(b)]. Considering now the constant density trajectories [dashed lines in Fig. 5(b)], it is apparent that while low density trajectories ($n_{e,ped}$=2, 4) have only a single intersection with the EPED prediction, high density trajectories (6,8) intersect the EPED prediction first at low pressure, and then twice more at higher pressure, corresponding to the 3 solutions in the inverted S-curve in Fig. 5(a).

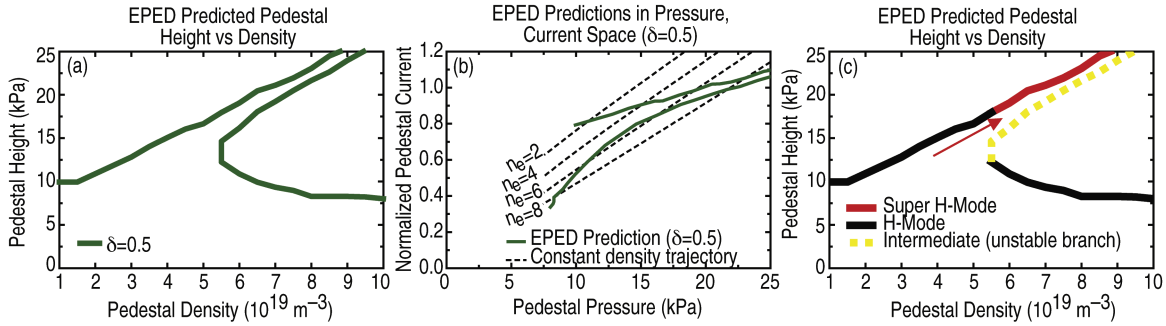

Fig. 5. (a) EPED predictions for the pedestal height (pressure in kPa) shown as a function of pedestal density for δ=0.5. The solution becomes multi-valued for pedestal density >5.5x10^{19} m^{-3}. (b) The same case from (a) is re-plotted in terms of pedestal current vs pedestal pressure. Trajectories of constant pedestal density are shown with dashed lines ($n_{e,ped}$=2, 4, 6, 8x10^{19} m^{-3}), indicating how the variation of current with density (collisionality), and the interaction of peeling-ballooning (+KBM) stability in pressure-current space, leads to the dependence shown in Fig. 5(a), including the presence of multiple roots at high density. (c) The same case as (a) with the Super H Mode, H-Mode and intermediate (dynamically unstable) pedestal roots labeled (red, black and dashed yellow, respectively). The red arrow indicates a parameter space trajectory by which the Super H regime can be accessed.

The interpretation of the three roots can be developed referencing Fig. 5(b). Note that the region above the top green line is inaccessible due to instability to current-driven modes, while the region below and to the right of the lower green line in inaccessible due to instability to pressure-driven modes. A trajectory starting at high density and low pressure (e.g. following an L-H transition or an ELM) will encounter the lower pressure solution, and stop (as it is now up against pressure driven instability limit). Hence this is the standard "H-mode" solution expected at that density. The uppermost solution can be reached only via dynamic variation of the density (or collisionality), starting at low values, and then increasing

with time. This is a robust (dynamically stable) solution, up against the current-driven mode limit. Because this solution exists above the standard H-mode solution at a given density, we refer to it as the "Super H-mode" solution. Finally, the intermediate root is dynamically unstable, as the pedestal will either rise from there to the Super H-mode solution (given the usual state of strong sources driving pedestal expansion), or, if it strongly encounters the pressure-driven instability boundary (eg due to a large ELM), it will drop to the H-Mode solution. The three separate solutions are labeled in Fig. 5(c). The red arrow in Fig. 5(c) indicates a density trajectory by which the Super H-Mode regime can be accessed. Note that trajectories which start at low pressure and increase pressure at constant density will always encounter the H-Mode solution first. Trajectories in which the density increases with pressure may partially enter into the Super H-mode region, though generally a dedicated effort to strongly increase the density (such as illustrated by the red arrow) is needed to deeply access the Super H-mode regime, and enter the space in which the Super H pedestal is more than twice the height of the H-mode pedestal at equivalent density.

The Super H-Mode regime exists whenever the plasma shaping, in combination with the effects of aspect ratio and q_{95}, are strong enough to lead to multiple crossings of constant density trajectories with the EPED solution, as in Fig. 5(b). For standard aspect ratio tokamaks, this typically occurs at triangularities $\gtrsim$0.4, but has a strong dependence on q_{95}. In some cases, the Super H-Mode regime exists only at densities higher than the Greenwald density limit. Super H-Mode raises a very interesting question about the physics of the Greenwald limit. Because collisionality scales with $n/T^2 \sim n^3/p^2$, the Greenwald limit will generally be reached at far lower collisionality in the Super H-Mode regime than in standard H-Mode (as p^2 is typically larger by a factor of 4 or more, at a given density, in Super H-Mode than in H-Mode).

4. Super H-Mode in DIII-D

As noted above, dynamic variation of the density, starting at low values and systematically increasing to values above the Super H-mode density threshold, should enable access to the Super H-Mode regime. The substantially higher pedestal pressure in Super H-Mode is expected to enable very high confinement, and also to increase global beta limits, due to the broadening of the pressure profile.

A recent set of experiments on DIII-D has successfully accessed the Super H-Mode regime, as described in Ref. 9. The initial experiment used parameters similar to the calculations in Fig. 5, B_t~1.9 T, I_p=1.5 MA, R=1.66 m, a=0.6 m, elongation=1.89, Z_{eff}~2.7, δ~0.5, β_N~1.8. The plasma was initiated at low density, and, following the L-H transition, the density was systematically raised via feedback control of the line average density, varying gas puffing rates. This allowed a trajectory through parameter space similar to that shown by the red arrow in Fig. 5(c). The observed pedestal height and density at 5 times are shown in Fig. 6, compared to EPED predictions. Good agreement is found between the predicted and observed pedestal height as the density is increased (t=1.7, 2.9, 3.5, 3.7 s), with access to the Super H-Mode regime at times ~3.5-3.7 s. After the onset of a core-tearing mode, the discharge falls into ELMing H-mode (4.3 s point in Fig. 6). Note the clear existence of two separate (Super H-mode and H-mode) pedestal regimes at high density, comparing 3.5-3.7 s with 4.3 s). [Note that the EPED predictions here use fixed values for the EPED inputs, which vary slightly in time in the experiment, and hence this comparison is not as precise as a full timeslice by timeslice comparison with the model, which shows better agreement].

These experiments were conducted with a quiescent (QH-Mode) edge, to enable a smooth trajectory through parameter space, uninterrupted by ELMs. Note that the term "QH Mode" describes a particular steady, quiescent edge condition with no ELMs, while the terms

"H-Mode" and "Super H-Mode" here describe particular pedestal roots in the parameter space of Figs 5 and 6. A QH mode edge may exist in either the H-mode regime or the Super H-Mode regime (the latter could be called QSH mode, though we do not use that terminology here). Note that a quiescent (QH) edge is predicted and observed to require operation near the current-driven stability boundary [10-12], which corresponds to the uppermost line in Fig. 6 (which the observations follow from t=1.7-3.7 s, while the edge is quiescent). At 4.3 s, after the pedestal falls to the lower H-Mode solution, where it is limited by pressure-driven instabilities, the QH edge is lost and ELMs return, consistent with expectations.

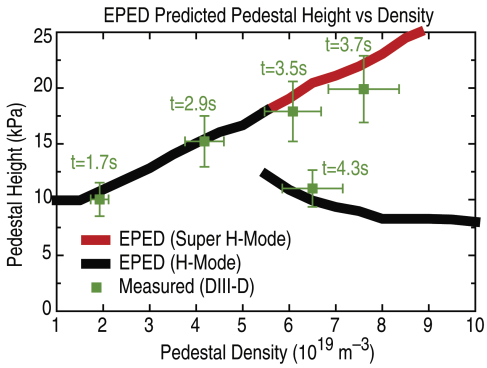

Fig. 6. Measured pedestal height and density (green squares) from a time sequence in DIII-D shot 153440 is compared to EPED predictions (red and black lines). Good agreement is found, with clear indication of both Super H-Mode (t=3.5-3.7 s) and H-Mode (t=4.3 s) pedestal roots at high density.

The experiments described above explored pedestal variation with density and access to Super H-mode, but did not attempt to fully take advantage of the very high Super H-Mode pedestal to enhance global performance. Feedback control of the global β_N was used in these experiments to maintain steady conditions, but this prevented the core pressure from rising with the pedestal to potentially achieve high global performance.

A very recent set of experiments were conducted on DIII-D to begin to explore both pedestal and core performance optimization in Super H-Mode. In these experiments, the core pressure is allowed to increase as the pedestal rises toward the Super H-mode regime via increasing density. A preliminary analysis of these experiments indicates that they have achieved a record high value of the global β_N (~3.1) for operation with a quiescent edge. Simultaneously they have achieved very high confinement, H_{98}>~1.2, more than 50% higher than typical H-mode values of H_{98}~0.7-0.8 at similar density, resulting in high normalized fusion performance. Analysis of these results, and planning for future experiments is ongoing, and further details will be reported in the future.

5. Discussion and Prospects for ITER

The predicted existence of the Super-H Mode regime, with substantially higher pedestal pressure than the equivalent H-Mode regime, creates a prospect for significant improvements in tokamak fusion performance. The recent experimental discovery of, and sustained operation in, the Super H-mode regime on DIII-D enhances those prospects substantially. Observations in Super H-Mode experiments on DIII-D, and H-mode experiments on several devices, are in generally good agreement with theoretical predictions from the EPED model, enhancing confidence that this model can be used to optimize the pedestal on ITER and DEMO, including access to Super H-mode at high density. Ongoing improvements in the EPED model should further improve its accuracy, particularly its ability to fully incorporate the effect of multiple impurity species. Additional theory and modeling development beyond the static EPED model is also underway to better understand pedestal dynamics, including the dynamical evolution of density, temperature, and rotation profiles. Super H-Mode experiments on DIII-D have thus far used a quiescent (QH) edge to enable smooth transit through pedestal parameter space and access to the Super H regime. It remains an open question whether a quiescent edge is necessary, or whether Super H-mode can be robustly accessed in ELMing plasmas. While plasmas with very large ELMs are likely only able to transiently access the Super H regime, it is possible that plasmas with small ELMs, such as pellet-driven

ELMs, may be able to robustly remain in Super H-mode.

Super H-mode access is predicted for ITER, and for DEMO concepts with high triangularity. The predicted Super H-mode parameter space for an ITER baseline case (B_t=5.3 T, I_p=15 MA, R=6.2 m, a=2.0 m, elongation=1.85, Z_{eff}~2, δ=0.485, β_N~2) is shown in Fig. 7. Super H-mode access at 15 MA is predicted for $n_{e,ped}Z_{eff}^{1/2}$ above ~$1.6x10^{20}m^{-3}$, or equivalently $n_{e,ped}$ above ~$1.2x10^{20}m^{-3}$ for Z_{eff}~2, which is near the Greenwald limit. As noted above, the pedestal collisionality in Super H-Mode at the Greenwald limit is far less than the pedestal collisionality in H-mode at the same density, and so Super H-mode operation offers an opportunity to explore the physics of the Greenwald limit, and perhaps even to exceed the limit, if Greenwald limit physics is related to collisionality.

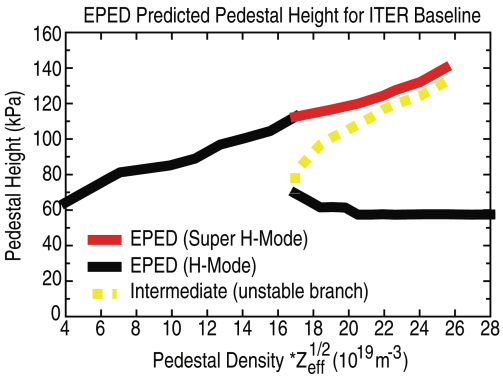

Fig. 7. EPED predictions for ITER baseline indicate a pedestal height increasing with density at moderate density, and potential Super H-Mode access (red line), with very high pedestal pressure, at high values of the product of density and square root of Z_{eff}.

We further note that the effect of collisionality on the bootstrap current is impacted by impurity concentration as well as density. The EPED calculations in Figs 4 through 6 were done at constant impurity concentration (constant values of Z_{eff}), and hence $n_{e,ped}$ can be used on the x-axis as a marker for collisionality (at a given pressure). When Z_{eff} is varied, the metric $n_{e,ped}Z_{eff}^{1/2}$ provides a useful figure of merit, as in Fig. 7, which indicates that ITER pedestal height and access to Super H-Mode can be improved by seeding low-Z impurities. Indeed injection of low Z impurities in the edge of ITER could provide a promising avenue both for protecting the divertor and enhancing pedestal, and global, performance.

Super H-mode access is predicted for a wide range of conditions on DIII-D, and experiments are planned to further explore this regime. Observations in very recent Super H-Mode experiments, including record values of β_N with a quiescent edge, in conjunction with high confinement, strongly encourage further study. Efforts are planned to further optimize Super H-Mode performance, including optimization of the coupled core-pedestal system, and to sustain it for longer durations.

This material is based upon work supported in part by the U.S. Department of Energy, Office of Science, Office of Fusion Energy Sciences, Theory Program, using the DIII-D National Fusion Facility, a DOE Office of Science user facility, under Awards DE-FG02-95ER54309 and DE-FC02-04ER54698, DE-AC02-09CH11466, DE-FG02-92ER54141, and DE-FC02-06ER54873.

References

[1] P.B. Snyder, *et al.*, Nucl. Fusion **51**, 103016 (2011)
[2] P.B. Snyder, *et al.*, Phys. Plasmas **19**, 056115 (2012)
[3] P.B. Snyder, *et al.*, Nucl. Fusion **49**, 085035 (2009); P.B. Snyder, *et al.*, Phys. Plasmas **16**, 056118 (2009)
[4] M. Beurskens, *et al.*, Phys. Plasmas **18**, 056120 (2011); M. Leyland *et al.*, Nucl. Fusion **53**, 083028 (2013)
[5] J.R. Walk *et al.*, Nucl. Fusion **52**, 063011 (2012); J.W. Hughes *et al.*, Nucl. Fusion **53**, 043016 (2013)
[6] R.J. Groebner *et al.*, Nucl Fusion **53**, 093024 (2013); R.J. Groebner *et al.*, Nucl. Fusion **50**, 064002 (2010)
[7] D.M. Orlov, invited talk APS DPP (2013); R. Nazikian et al., oral G04.0004 APS DPP (2013).
[8] E.A. Belli and J. Candy, Plasma Phys. Control. Fusion **54**, 015015 (2012)
[9] W.M. Solomon, P.B. Snyder, K.H. Burrell, *et al.*, "Access to a new plasma edge state with high density and pressures using quiescent H-mode," to appear in Phys. Rev. Lett. (2014).
[10] K.H. Burrell, *et al.*, Nucl. Fusion **49**, 085024 (2009)
[11] P.B. Snyder, *et al.*, Nucl. Fusion **47**, 961 (2007).
[12] T.H. Osborne, *et al.*, J. of Physics: Conference Series **123**, 012014 (2008).